sciendo

Polish Journal of Chemical Technology, 25, 4, 52—60, 10.2478/pjct-2023-0038

Study on safe disposal of cephalosporins based on kinetic pyrolysis mechanism

Jiangxue Fan[1, 2], Meng Zhang[1, 2], Xiaofei Hou[1, 2], Fang Wang[1, 2], Mengyuan Bai[1, 2], Ruoxi Jiao[1, 2], Zhongyu Yang[1, 2*], Erhong Duan[1, 2*], Fengfei Cheng[3], Wen Zhou[4]

[1]School of Environmental Science and Engineering, Hebei University of Science and Technology, Shijiazhuang, Hebei 050018, PR China
[2]National and Local Joint Engineering Center of Volatile Organic Compounds & Odorous Pollution Control Technology, Shijiazhuang, Hebei 050018, PR China
[3]Hebei provincial pollutant emission rights trading service center, Shijiazhuang, Hebei 050000, PR China
[4]The State Grid Hebei Electric Power Company Electric Power Research Institute, Shijiazhuang, Hebei, 050021, PR China
[*]*Corresponding authors: e-mail:* yzyzhongyuyang@163.com; duan_eh@163.com

Based on the global goals for cleaner production and sustainable development, the pyrolysis behavior of cephalosporin residues was studied by TG-MS method. The influence of full temperature window on the safe disposal of residues was analyzed based on the "3-2-2" and "1+1" of thermal analysis kinetics, and the gas by-products of thermal degradation were monitored. Results showed that the pyrolysis of distillation residues were divided into low and high-temperature zones, including six stages. Maximum error rate (8.55%) by multiple scan rate was presented based on "3-2-2" pattern and maximum total fluctuation (33.7) by single scan rate was presented based on "1+1" pattern, which implied that the comprehensive multi-level comparison method was very reliable. The E value "E" of six stages showed an increasing trend ranging 166.8 to 872.8 kJ/mol. $\mathrm{Lg}A_{(\mathrm{mean})}$ was 27.28. Most mechanism function of stage 1, 2 were Z-L-T equation (3D), stage 3, 4, 6 were Avrami-Erofeev equation (AE3, AE4, AE2/3) and stage 5 was Reaction Order (O2). In addition, various small molecular micromolecule substances were detected such as C_2H_4O, C_2H_6, NH_3, CH_4, CO_2 under full temperature windows and a possible pyrolysis path of residues was provided.

Keywords: Distillation residues; Thermal analysis kinetics; "3-2-2"; "1+1"; Pyrolysis mechanism.

INTRODUCTION

China is the world's largest producer of antibiotic raw materials and produces 80% of the cephalosporins. The main characteristics of antibiotics are the variety of products, the use of raw and auxiliary materials, the generation of pollutants, the production process is complex, and the treatment process and discharge methods are diversified. The residual antibiotics in the residues of bacteria can induce the production of resistance genes and cause drug resistance of bacteria[1, 2, 3]. If improperly handled, it is easy to cause the spread and diffusion of drug-resistant bacteria, which endangers the ecological environment and human health. In 2008, China listed fermented pharmaceutical residues in the List of Hazardous Wastes[4]. The technology and equipment for the efficient and safe conversion of cephalosporin residue from organic distillation and the utilization of materials and energy are not only the focus of pollution in the pharmaceutical industry but also the difficulty of control, which has become the bottleneck restricting the sustainable development of the pharmaceutical industry.

High-temperature pyrolysis is the use of heat energy to cut off the chemical bonds in macromolecules and transform them into non-toxic and harmless small molecular substances under the condition of isolating air or passing into a small amount of air[5]. Meanwhile, pyrolysis of distillation residues based on high-temperature treatment can obtain products with rich pore structure, unique morphology, excellent adsorption or electrochemical properties. However, the reaction of the high-temperature treatment process is ambiguous, and the synthesis path of the by-product is not clear, which indicates that the pyrolysis mechanism cannot be determined. This inhibits the development of high-temperature pyrolysis technology for the safe disposal of solid waste.

It is understood that specific mathematical models are widely used in the kinetic analysis of material mechanisms. Thermal analysis kinetics were usually used to analyze the high-temperature treatment mechanism of materials by the calculation for kinetic triplet ($G(\alpha)$, E and A)[6, 7, 8, 9]. The mechanism microscopic shows the fracture and formation of the bond of the whole reaction process. By using C-R thermal analysis kinetics, Wu Di et al. calculated the average activation energies of the three decomposition stages of ammonium sulfate and the most probable mechanism functions to provide a theoretical basis for the full utilization of ammonium sulfate[10]. Wu Xinrong et al. obtained the average activation energy values using Starink, FWO and Kissinger methods, and concluded that the activation energy is small and the combustion chemical reaction is easy to occur[11]. Zhu Wei et al. used Arrhenius thermal analysis kinetics to calculate the activation energy which concluded that the reaction activation energy slag wax C > slag wax D > slag wax B[12]. Although many mathematical models were used to calculate the kinetic parameters, the accuracy of the results may appear contingency, creating a bias of a single calculation method. It is understood that specific mathematical models are widely used in the kinetic analysis of material mechanisms, in this paper, "3-2-2" and "1+1" models were used to more accurately infer the pyrolysis mechanism and kinetic parameters by comparing the differential and integral results of the same mechanism function which were more conducive to the analysis of the overall reaction kinetics "1+1" was the pattern based on the contrast of C-R and ABSW by comparing the minimum of total volatility Δ total.

"3-2-2" was the pattern of multiple-level comparison of three models (FWO, KAS, Starink) of E-G(α), two models (Popescu, Friedman) of G(α)-E and two calculation ways (E-G(α), G(α)-E). A thermogravimetric analyzer was used together with the mass spectrometer detector (TG-MS) to acquire the information on gas by-products in real time[12, 13] in the process of analyzing the relationship between quality and temperature for exploring the reaction path.

To achieve safe disposal, the thermal analysis kinetic method based on the "3-2-2" and "1+1" modes were utilized to analyze the possible degradation mechanism of cephalosporin residue. According to the pyrolysis characteristics of organic residues, the data of temperature as a function of mass were obtained. TG/DTG curve was used to study the pyrolysis characteristics of organic residues, and the deep mechanism of high-temperature degradation of organic residues was inferred, which provided the possibility for the clean production or sustainability of cephalosporin pollutants in China.

MATERIALS AND METHODS

Preparation of materials

The materials (residues of distillation organic kettle) were obtained from a cephalosporin pharmaceutical factory. It was centrifuged and dried at 80 °C for 12 hours, then put it into centrifugal pipe in desiccator for standby.

Characterization of materials

The distillation residues were analyzed using an X-ray diffractometer manufactured by D/Max-2500 (Rigaku Corporation, Japan) with Cu Kα radiation (λ = 0.15406 nm). The scanning electron microscope (SEM) measurements were presented by using the Prisma-E (Thermo Fisher Scientific).

Thermogravimetric text

The pyrolysis of distillation residues was performed in NETZSCH STA 449 F5/QMS 403 D thermogravimetric mass spectrometer (NETZSCH, Germany). At the heating rates of 5, 10, 15, 20, 25 K/min ranging from 323 to 1273 K with an He flow of 40 mL/ min, distillation residue of 5 ± 0.3 mg was added into the alumina crucible with lid of Pt-Rh and pyrolyzed to obtain the data involving temperature and quality. Whether the TG curves at different heating rates are similar in general indicates whether the experiment has certain reliability and repeatability. The gas by-products produced during the pyrolysis process were acquired by the mass spectrometer to get possible paths of material pyrolysis. The experimental device diagram is shown in Fig. 1.

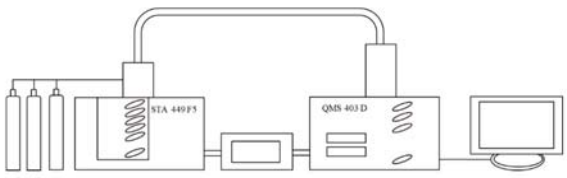

Figure 1. The diagram of experiment equipment.

Study of thermal analysis kinetics

The possible combustion mechanism of organic bacterial residue was calculated and analyzed by using two different modes of thermal analytical kinetics "3-2-2" and "1+1". The reaction activation energy E can provide A basis for the heat required for high-temperature treatment, the pre-factor A can predict the reaction trend, and the most likelihood mechanism function G(α) can predict the combustion mechanism. The data about the mass and temperature of materials were used in the kinetic calculation process. The conversion rate ranging from 0.2-0.8 with the steps of 0.05 was selected to calculate the three factors of kinetics (G(α), E and A).

Single scan rate methods

Coats-Redfern (C-R)[14, 15] and Achar-Brindley-Sharp--Wendworth (ABSW)[16] models were used to solve the kinetic triplet of pyrolysis distillation residues.

The formulas of C-R and ABSW were listed as follows:

$$\ln\left[\frac{\mathrm{G}(\alpha)}{T^2}\right] = \ln\left(\frac{A\mathrm{R}}{\beta E}\right) - \frac{E}{\mathrm{R}T} \ (\mathrm{C-R}) \tag{1}$$

$$\ln\left[\frac{\beta \mathrm{d}\alpha}{\mathrm{d}T}\right] = \ln A - \frac{E}{\mathrm{R}T} \ (\mathrm{ABSW}) \tag{2}$$

Where f(α) and G(α) represented the differential and integral forms of the kinetic model function, respectively; T was reaction temperature, K; R was the gas constant, 8.314 J/(mol · K); β was the heating rate, K/min; E was the apparent activation energy, kJ/mol; A was the pre-exponential factor, min^{-1}.

The E and A values were calculated by the slope and intercept of the regression line from fitting $\ln[\mathrm{G}(\alpha)/T^2]$ vs $1/T$ (C-R) and $\ln[(\beta \mathrm{d}\alpha/\mathrm{d}T)/\mathrm{f}(\alpha)]$ vs $1/T$ (ABSW). G(α) were acquired by screening the ones with high linearfitting by comparison.

Multiple scan rate methods

The multiple scan rate method was widely used by domestic and foreign scholars because it avoided on the selection of the most probable mechanism function to obtain more reliable E values through comparing with single scan[7, 17]. In this paper, five models based on the different calculation order of E and G(α) were divided into two calculation ways marked as E-G(α) (FWO, KAS, Starink) and G(α)-E (Popescu, Friedman). Multiple-level comparison of three models, two models and two calculation ways were introduced as "3-2-2".

(1) E-G(α)

Flynn-Wall-Ozawa (FWO)[18, 19], Kissinger-Akahira-Sunose (KAS)[12, 20] and Starink[21, 22] models were used in the way of E-G(α). The E values were first calculated by FWO, KAS and Starink three ways.

The formulas of FWO, KAS, and Starink were presented as follows:

$$\ln\beta = \ln\frac{0.0048AE}{\mathrm{R}\mathrm{G}(\alpha)} - 1.0516\frac{E}{\mathrm{R}T} \ (\mathrm{FWO}) \tag{3}$$

$$\ln\left(\frac{\beta}{T^2}\right) = \ln\frac{A\mathrm{R}}{E\mathrm{G}(\alpha)} - \frac{E}{\mathrm{R}T} \ (\mathrm{KAS}) \tag{4}$$

$$\ln\left(\frac{\beta}{T^{1.8}}\right) = \mathrm{C_s} - 1.0037\frac{E}{\mathrm{R}T} \ (\mathrm{Starink}) \tag{5}$$

Under the TG curve with different heating rates, the E values were calculated through the slope of the regression line from fitting $\ln\beta$ vs $1/T$ (FWO), $\ln[\beta/T^2]$ vs $1/T$ (KAS) and $\ln[\beta/T^{1.8}]$ vs $1/T$ (Starink), respectively.

The second step, $G(\alpha)$ and the A values could be calculated based on the above E value involving the integral master-plot method[23] and Tang-Liu-Zhang-Wang-Wang temperature integral approximation.

The formulas of the integral master-plot method and Tang-Liu-Zhang-Wang-Wang temperature integral approximation were expressed as follows:

$$G(\alpha) = \int_{T_0}^{T} \left(\frac{A}{\beta}\right) \exp\left(-\frac{E}{RT}\right) dT \approx \int_{0}^{T} \left(\frac{A}{\beta}\right) \exp\left(-\frac{E}{RT}\right) dT = \left(\frac{AE}{\beta R}\right) P(u) \quad (6)$$

$$\frac{G(\alpha)}{G(0.5)} = \frac{P(u_\alpha)}{P(u_{0.5})} \quad (7)$$

$$P(u_\alpha) = \frac{e^{-u_\alpha}}{u_\alpha - (1.00198882u_\alpha + 1.87391198)} \quad (8)$$

The experiment master-plots and theoretical master-plots could be obtained by fitting P (α)/P (0.5) vs α and G (α)/G (0.5) vs α. The $G(\alpha)$ could be obtained by comparing the shape of the experimental master-plots with the theoretical master-plots.

(2) $G(\alpha)$-E

Popescu-Friedman models were used in the way of $G(\alpha)$-E. The $G(\alpha)$ was first screened by Popescu[24] model. The more reliable E values were acquired by the comparison of Friedman[25] and Popescu models.

The formula of Popescu was performed as follows:

$$G(\alpha)_{mn} = \frac{1}{\beta} I(T)_{mn} \text{ (Popescu)} \quad (9)$$

Under the different heating rates, the data of (T_m, T_n) and (α_m, α_n) were collected. In the reasonable range of β and α values, the $G(\alpha)_{mn}$ vs $1/\beta_i$ relationship was a straight line passing through the coordinate origin. If the experimental data and the adopted $G(a)$ met the above straight line, the $G(a)$ was the kinetic mechanism function reflecting the real chemical process.

In the second step, the E, A values of Popescu model and the E value of Friedman model were calculated.

The formulas of Popescu and Friedman were performed as follows:

$$\ln\left(\frac{\beta}{T_n - T_m}\right) = \ln\left[\frac{A}{G\ \alpha)_{mn}}\right] - \frac{E}{RT_\zeta} \text{ (Popescu)} \quad (10)$$

$$\ln\left(\frac{\beta d\alpha}{dT}\right) = \ln Af(\alpha) - \frac{E}{RT} \text{ (Friedman)} \quad (11)$$

The E and A values of Popescu were calculated through the slope and intercept of the regression line from fitting $\ln[\beta/(T_m - T_n)]$ vs $1/T_\zeta$. The E values of Friedman model were calculated through the slope of the regression line from fitting $\ln(\beta d\alpha/dT)$ vs $1/T$.

RESULTS AND DISCUSSION

Characterization of materials

The photo file of distillation residues with orange powder is shown in Fig. 2. The SEM images are presented in Fig. 3. It could be seen from Fig. 3 (A) that the distillation residual solids were lumpy substance. After amplification, it was observed that solids were built by the accretion of numerous nanoparticles with sizes ranging from tens to 200 nm (Fig. 3 (B)). The XRD patterns of rectification residues are shown in Fig. 4. The three possible substances were presented with comparison results based on the characteristic diffraction peak. According to the spectrum library comparison results, the rectification residue may contain #72-1668 NaCl, NaCNO(#44-0770), $C_4H_3KO_8 \cdot 2H_2O$ (#31-1029).

Figure 2. The photo file of distillation residues

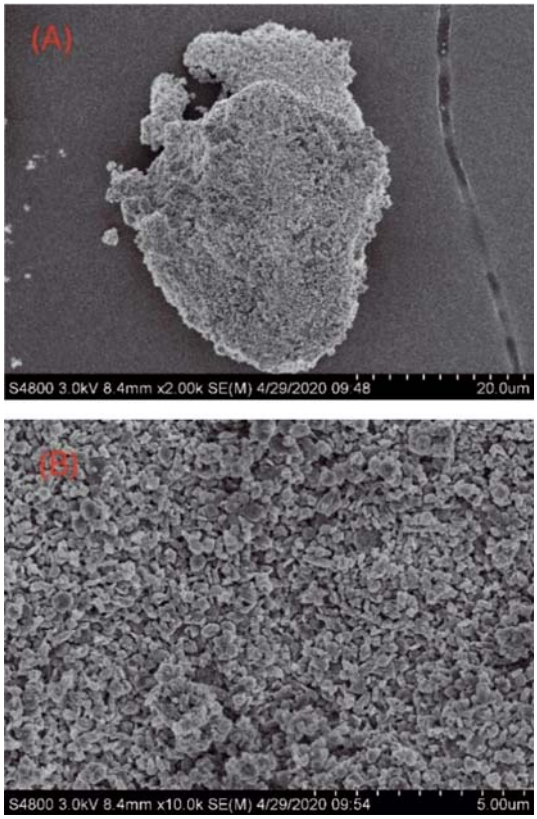

Figure 3. SEM image for distillation residues: 20 μm (A) and 5 μm (B)

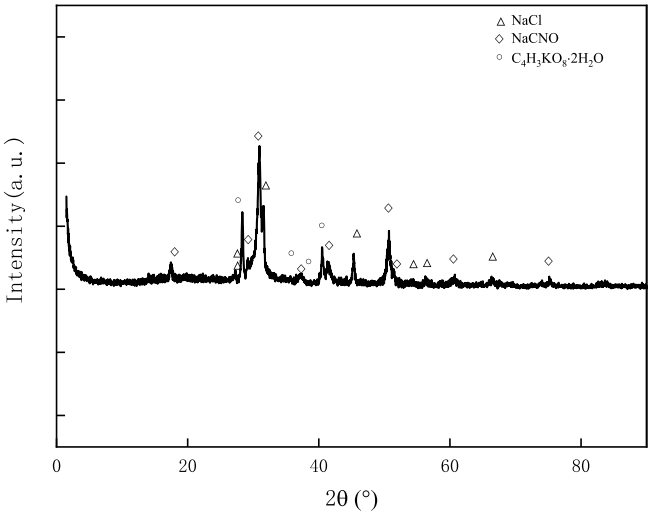

Figure 4. XRD pattern for distillation residues

Analysis of pyrolysis characteristics

It is important to analyze pyrolysis characteristics of residues based on the data of temperatures vs mass, which is good for estimating the change of the solid waste with temperatures and preliminarily determining possible reactions in the process for the calculation of thermal analysis kinetics. The TG and DTG curves which measured the distillation residues by TG-MS under the He atmosphere were shown in Fig. 5. The TG curves generally presented similarity with different heating rates, which indicated that the experiment had certain reliability and repeatability. There were also some unique differences in part, which was the low-temperature range had a high coincidence degree but the high-temperature range had a deviation. Coincidence may be due to less energy required for the current reaction. The deviation may be the thermal hysteresis phenomenon or heat conduction of materials[26, 27]. With the increase of heating rate, the time for the material to obtain heat energy was shortened. Although required temperature of surface could reach, inside temperature of material was not enough to required energy for the reaction. The DTG curves showed obvious "hollow" at the same heating rate and "stratification" at different heating rates, indicating different reaction types and intensities. The low and high-temperature regions were divided into six stages based on the "hollow" of DTG. The weight loss rates of each stage are presented in Table 1. The weight loss of the first major part was 23.10% and the second major part was 53.19% accounting for 98.5% of the total weight loss, which showed two zones including six stages were selected as the main thermal analysis stage from TG / DTG curves. In the six stages, stages 1, 2, 5, 6 reacted violently and stages 3, 4 reacted genteelly, which may be due to stage 3 and stage 4 being the transition stages. It is noted the reaction of high-temperature pyrolysis was ambiguous for the safe disposal of distillation residues explored for the first in the work. Moreover, the method of high-temperature heat treatment can not only promote the decomposition of solid waste and reduce toxicity, such as determining the best treatment temperature according to the optimal growth conditions of chlorella, but also generate new valuable products such as carbon materials, which have been applied in the field of adsorption separation[28], catalysis[29], energy storage[30] and conversion[31]. However, the synthesis of most products was only presented by a simple process of high-temperature pyrolysis carbonization[32, 33], which showed that the possible reaction mechanism was not clearly stated. To further explore the pyrolysis mechanism of residues in high-temperature treatment process, thermal analysis kinetics were used by the calculation for kinetic triplet (G(α), E and A).

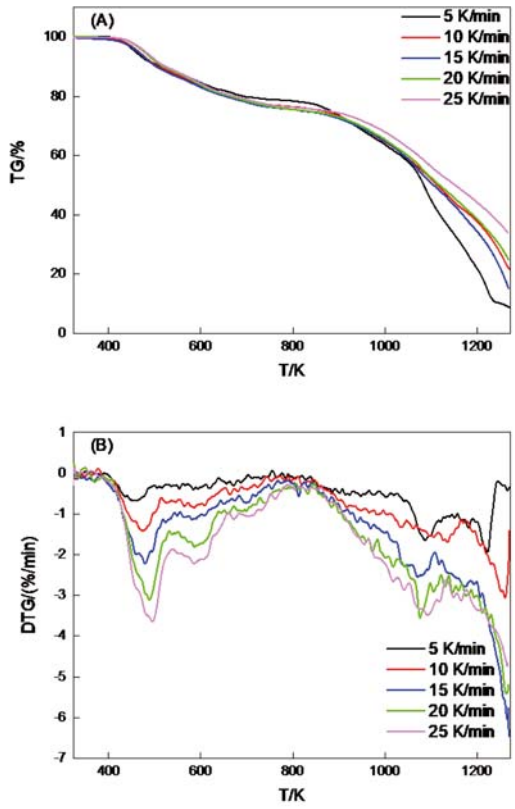

Figure 5. TG (A) and DTG (B) curves for material at different heating rates

Table 1. Percentage of weight loss at low and high-temperature stage of materials

β K/min	low-temperature stage %	high-temperature stage %	total weight loss %
5	21.19	68.84	91.28
10	23.13	53.94	78.24
15	24.00	59.44	84.75
20	23.91	49.62	74.83
25	23.28	41.60	65.89
Average	23.10	54.69	79.00

Analysis of kinetic parameters

Commonly used mechanism functions combined with kinetic models were performed in Table 2. According to the characteristics of TG and DTG curves, the process can be divided into six stages. In all six stages, stages 1, 3 and 4 were calculated based on "3-2-2" from multiple rate methods and stages 2, 5 and 6 were calculated based on "1+1" from single rate methods. The comparison of *E*-G(α) (FWO, KAS, Starink) and G(α)-*E* (Popescu, Friedman) were applied from "3-2-2" for the calculation of kinetic parameters. The comparison based on "1+1" was presented by C-R and ABSW.

Table 2. Most commonly used kinetic mechanism function

No.	Function name	Symbol	G(α)	f(α)
1	Jander equation	2D	$[1-(1-\alpha)^{1/2}]^2$	$(1-\alpha)^{1/2}[1-(1-\alpha)^{1/2}]^{-1}$
2	Jander equation	D_3	$[1-(1-\alpha)^{1/3}]^2$	$3/2(1-\alpha)^{2/3}[1-(1-\alpha)^{1/3}]^{-1}$
3	Z-L-T equation	3D	$[(1-\alpha)^{-1/3}-1]^2$	$3/2(1-\alpha)^{4/3}[(1-\alpha)^{-1/3}-1]^{-1}$
4	Avrami-Erofeev equation	$A_{1.5}$	$[-\ln(1-\alpha)]^{2/3}$	$3/2(1-\alpha)\,[-\ln(1-\alpha)]^{1/3}$
5	Avrami-Erofeev equation	$A_{4/3}$	$[-\ln(1-\alpha)]^{3/4}$	$4/3(1-\alpha)\,[-\ln(1-\alpha)]^{1/4}$
6	Mampel Single-line rule	A_1,F_1	$-\ln(1-\alpha)$	$1-\alpha$
7	Avrami-Erofeev equation	$A_{2/3}$	$[-\ln(1-\alpha)]^{3/2}$	$2/3(1-\alpha)\,[-\ln(1-\alpha)]^{-1/2}$
8	Avrami-Erofeev equation	AE_3	$[-\ln(1-\alpha)]^3$	$1/3(1-\alpha)\,[-\ln(1-\alpha)]^{-2}$
9	Avrami-Erofeev equation	AE_4	$[-\ln(1-\alpha)]^4$	$1/4(1-\alpha)\,[-\ln(1-\alpha)]^{-3}$
10	Reaction order	O_1	$1-(1-\alpha)^{1/4}$	$4(1-\alpha)^{3/4}$
11	Contraction sphere (volume)	R_3	$1-(1-\alpha)^{1/3}$	$3(1-\alpha)^{2/3}$
12	–	3D	$3[1-(1-\alpha)^{1/3}]$	$(1-\alpha)^{2/3}$
13	Reaction order	O_2	$(1-\alpha)^{-1}-1$	$(1-\alpha)^2$

Analysis of stage 1

Firstly, "Pattern 3" was applied in E-G(α) method with FWO, KAS, Starink models. As shown in T able S1, the E values of the three models are very close, approximately ranging from 130 to 300 kJ/mol (α = 0.2–0.8). Fitting degree of R^2 values were relatively high, all above 0.94. The average E values of three models were 161.48, 161.95, 162.14 kJ/mol and the error rate were 0.23%, 0.06%, 0.17%, respectively. There were also some special phenomena. The E values presented an increasing trend with the increase of the conversion rate, which hinted that this stage was a multi-step combination reaction. The fluctuation difference of E value was 178.98 kJ/mol. This may be due to the production of intermediate. R^2 values were increased from 0.94 to 0.99 with the rise of the conversion rate. It can be seen in Fig. S1 that the fitting curves "focused" to the upper left.

The E values of FWO, KAS and Starink models were respectively substituted into the equation (8) to obtain different temperature integral $P(u_\alpha)$. It could be seen from Fig. S2, that the shape of the experimental mater-plots was similar at different heating rates, which indicated that the heating rates did not affect the calculation of the pyrolysis mechanism of distillation residues. Therefore, the experimental master-plots at the 10 K/min heating rate was taken as an example to compare with the theoretical master-plots. The comparison between the experimental master-plots and the theoretical master-plots of stage 1 is shown in Fig. S3. By comparing the experimental master-plots and the theoretical master-plots of three models, the experimental master-plot of stage 1 was matched to the theoretical master-plot Z-L-T equation.

The Z-L-T equation was substituted into Equation (8):

$$G(\alpha) = \left(\frac{AE}{\beta R}\right) P(u) = [(1-\alpha)^{-\frac{1}{3}} - 1]^2 \quad (12)$$

The R^2 of kinetic index correction values can be acquired by fitting $[(1-\alpha)^{-\frac{1}{3}} - 1]^2$ vs $\left(\frac{E}{\beta R}\right) P(u_\alpha)$ and A value from the slope value (Fig. S4).

Then, for better comparison, "pattern 2" was quoted based on G(α)-E method by Popescu-Friedman models. In G(α)-E method, G(α) was first identified. As shown in Table S2, fitting result of Popescu model selection based on the maximal R^2 displayed that Z-L-T equation was the kinetic mechanism function. The E values of Popescu-Friedman were calculated according to the most probable mechanism function. It can be seen from Table S3 that the calculation of E values from two models had no obvious differences, which showed the calculation of Popescu model was reliable for analyzing the pyrolysis mechanism of stage 1. The average E values were 181.81, 202.48 kJ/mol and the error rates were 5.38%, 5.38%, respectively.

Finally, the last "pattern 2" in "3-2-2" was presented by the comparison two calculated ways based on E-G(α) and G(α)-E. The comparison of mechanism functions between two calculated ways showed that the E and A values of the different models were similar, the R^2 values were high (above 0.94) and most mechanism functions were the same. These showed E-G(α) and G(α)-E two methods were reliable to obtain kinetic parameters of stage 1. The obtained kinetic parameters of the stage 1 pyrolysis process are listed in Table S4. It could be seen that the $E_{(mean)}$ of stage 1 was 177.00 kJ/mol and the error rate respectively were 8.55% and 8.56%, the LgA value was 17.13 min^{-1}, and the most mechanism function was Z-L-T equation. The reaction mechanism of Z-L-T equation was 3D.

Analysis of stage 2

For stage 2, kinetic parameters were calculated by two different forms of kinetic models, respectively, in which C-R attributed to the integral form and ABSW attributed to the differential form (Fig. S5). The E values range from 73.1 to 321.9 kJ/mol. Optimal kinetic parameters were chosen by "1+1", which was based on the assessment criteria (The value of R^2 was closer to 1 and total fluctuation of ΔLgA and ΔE). As shown in Table S5, the most probable mechanism was No.3 (Z-L-T equation of 3D) due to better fitting (R^2 = 0.99) and minimum total fluctuation (ΔLgA = 8.2, ΔE = 2.5). The Value of $E_{(mean)}$ was 176.0 kJ/mol. The Value of $Lg A_{(mean)}$ was 8.8 min^{-1}.

Analysis of stage 3

"Pattern 3" was used firstly based on E-G(α) method. In this method, the E values of the three models were very close, ranging from 300–700 kJ/mol. The R^2 of conversion rate below 0.7 was greater than 0.94 and R^2 decreased with the increase of conversion rate, which may be due to the affect gentle based on DTG curves. The average E values of three models were 412.86, 422.43, 422.05 kJ/mol, and the error rate were 1.49%, 0.79%, and 0.70%, respectively (Table S6). Some special phenomena were also presented that the E values showed a trend of

decreasing first and then increasing, which hinted that this stage was a multi-step combination reaction. The fluctuation difference of E value was 401.37 kJ/mol. Contrary to the law of E values, R^2 generally showed a trend of increasing first and then decreasing. It can be seen in Fig. S6 that the fitting curves "focused" to the lower right.

The E values of FWO, KAS and Starink models were respectively substituted into the equation (8) to obtain $P(u_\alpha)$. The shape of the experimental mater-plots was presented in Fig. S7. The experimental master-plots at the 10 K/min heating rate were taken to compare with the theoretical master-plots, which was shown in Fig. S8. By comparing, the experimental master-plot of stage 3 was similar to the theoretical master-plot Avrami-Erofeev equation.

The Avrami-Erofeev equation was substituted into Equation (8):

$$G(\alpha) = \left(\frac{AE}{\beta R}\right) P(u) = -[\ln(1-\alpha)]^3 \quad (13)$$

The R^2 of kinetic index correction values could be acquired by fitting $[(1-\alpha)^{-\frac{1}{3}} - 1]^2$ vs $\left(\frac{E}{\beta R}\right) P(u_\alpha)$ and the A values were the slope values (Fig. S9).

"Pattern 2" was quoted based on G(α)-E method for better comparison. In G(α)-E method, as shown in Table S7, fitting result of Popescu model displays that Avrami-Erofeev equation was the kinetic mechanism function. It can be seen from Table S8 that the calculation E values of Popescu and Friedman models had no obvious differences, which showed the calculation of Popescu model was reliable. The average E values were 354.50, and 363.91 kJ/mol and the error rate was 1.31%, respectively.

In the last "pattern 2", a comparison of mechanism functions between the E-G(α) and G(α)-E two calculated ways showed that the E and A values of the different models were closed, the R^2 values were high and the most mechanism functions were the same. These showed E-G(α) and G(α)-E two methods were reliable to obtain kinetic parameters of stage 3. The obtained kinetic parameters of stage 3 pyrolysis process are listed in Table S9. It could be seen that the $E_{(mean)}$ of stage 3 was 389.16 kJ/mol and the error rate respectively were 7.70% and 7.70%, the LgA value was 29.49 min^{-1}, the most mechanism function was Avrami-Erofeev equation. The reaction mechanism of stage 3 was AE_3.

Analysis of stage 4

In the "pattern 3" of E-G(α) method, the E values of the three models were very closed, from 0.2–0.8 to about 380–1100 kJ/mol. R^2 values were relatively high, all above 0.92. The average E values of three models were 572.65, 586.25, 579.98 kJ/mol and the error rates were 1.22%, 1.13%, and 0.04%, respectively (Table S10). There were also some special phenomena. The E values an overall increasing trend with the increase of the conversion rate, which hinted that this stage was a multi-step combination reaction. The fluctuation difference of E value was 743.89 kJ/mol. R^2 ranged from 0.92 to 0.98. It can be seen in Fig. S10 that the fitting curves were "parallel".

The E values of FWO, KAS and Starink models were respectively substituted into the equation (8) to obtain $P(u_\alpha)$. The experimental mater-plots are presented in Fig. S11. The experimental master-plots at the 10 K/min heating rate were taken to compare with the theoretical master-plots (Fig. S12). By comparing, the experimental master-plot of stage 4 was similar to the theoretical master-plot Avrami-Erofeev equation.

The Avrami-Erofeev equation was substituted into Equation (8):

$$G(\alpha) = \left(\frac{AE}{\beta R}\right) P(u) = -[\ln(1-\alpha)]^4 \quad (14)$$

The R^2 of kinetic index correction values can be acquired by fitting $[(1-\alpha)^{-\frac{1}{3}} - 1]^2$ vs $\left(\frac{E}{\beta R}\right) P(u_\alpha)$ and the A values were the slope values (Fig. S13).

In "pattern 2" of G(α)-E method, the kinetic mechanism function of Popescu model was Avrami-Erofeev equation (Table S11). It could be seen from Table S12 that the calculation E values of Popescu and Friedman models were very close, which showed the calculation of Popescu model was reliable. The average E values were 661.19, 682.65 kJ/mol and the error rates were 1.60%, and 1.60%, respectively.

The last "pattern 2" comparison of mechanism functions between the E-G(α) and G(α)-E two calculated ways that the E and A values of the different models were closed, the R^2 values were high and the most mechanism functions were the same. These showed E-G(α) and G(α)-E two methods were reliable to obtain kinetic parameters of stage 4. The obtained kinetic parameters of stage 4 pyrolysis process are listed in Table S13. It can be seen that the $E_{(mean)}$ of stage 4 was 625.82 kJ/mol and the error rates respectively were 7.37% and 7.37%, the LgA value was 31.77 min^{-1}, the most mechanism function was Avrami-Erofeev equation. The reaction mechanism of stage 4 was AE_4.

Analysis of stage 5

In this stage, kinetic parameters were calculated by C-R and ABSW two models, respectively (Fig. S14). The choice of optimal kinetics parameters was same as stage 2. The most probable mechanism was No.13 (Reaction Order of O_2) due to better fitting (R^2 = 0.99) and minimum total fluctuation (ΔLgA = 8.5, ΔE = 25.2). The Value of $E_{(mean)}$ was 784.2 kJ/mol. The Values of Lg$A_{(mean)}$ was 36.3 min^{-1} (Table S14).

Analysis of stage 6

C-R and ABSW two models were used to calculate kinetic parameters, respectively (Fig. S15). It can be seen from Table S15 that the ΔE of No. 6, No. 7 and No. 9 were identical and the differences of ΔLgA were no obvious. No. 6, No. 7 and No. 9 were the probable mechanism. In combination with the previous stages, the E value tended to increase and the growth rate of each stage was about 100–200 kJ/mol. Therefore, No. 6 and No. 9 were excluded. The most probable mechanism was No. 7 (Avrami-Erofeev equation of $A_{2/3}$) due to better fitting (R^2 = 0.99) and minimum total fluctuation (ΔLgA = 9.8, ΔE = 0.9). The Value of $E_{(mean)}$ was 872.8 kJ/mol. The Value of Lg$A_{(mean)}$ was 36.1 min^{-1}.

In the materials pyrolysis processes, the mechanism functions of stage 1, 2 were all Z-L-T equation. Therefore, stage 1 and stage 2 could be divided into the

initial stage which possibly was the volatilization stage. The mechanism functions of stage 3, 4 as the transition stage all were Avrami-Erofeev equation (n = 3, 4). The mechanism function of stage 5 was Reaction Order. The Stage 5 possibly was the cracking stage. The mechanism function of stage 6 was Avrami-Erofeev equation. The stage 6 possibly was the carbonization stage. The growth rate of each stage was about 100–200 kJ/mol proving that the chemical bond energy of each stage increases steadily with little interval. The values of R^2 calculated by the C-R model were closer to 1 in all stages of the pyrolysis process compared with the ABSW model, which may deduce a result that the C-R model was more suitable for the kinetical analysis of the pyrolysis process of distillation residues. According to the analysis results, the calculation results of the kinetic parameters of the C-R, ABSW, FWO, KAS, Starink, and Popescu models were more suitable for analyzing the pyrolysis mechanism of materials. Though the mechanism of pyrolysis at high temperature has been clarified in detail, the data on by-products composition is indispensable due to the need for the combination of theory and practice (for example, harmful gases may be produced with the increase of temperatures, which needs effective measures to control[34]).

Mass spectrometry

Though high-temperature treatment of biopharmaceutical residues has not been reported, the effects of temperatures on changes in the gas composition were studied based on the pyrolysis of waste pharmaceutical blisters[35]. The data of by-products composition was obtained using TG-MS in the work. The mass spectrometry data was acquired from the thermogravimetric gas products information at 10K heating rate. Three-dimensional mass spectrograms of different mass Numbers were presented in Fig. 6. During the pyrolysis process, the by-product concentration changes were obvious, which mainly concentrated in m/z = 10–50 (Fig. 6). As shown in Fig. 7(A), C_2H_4O (m/z = 44) were observed ranging from 393–773 K (stage 1, 2, 3). It could be seen from Fig. 7(B) that C_2H_6 (m/z = 30) was detected ranging

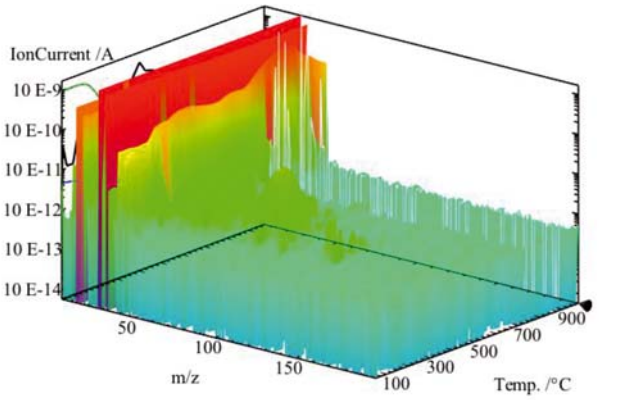

Figure 6. Three-dimensional mass spectrograms of different mass Numbers

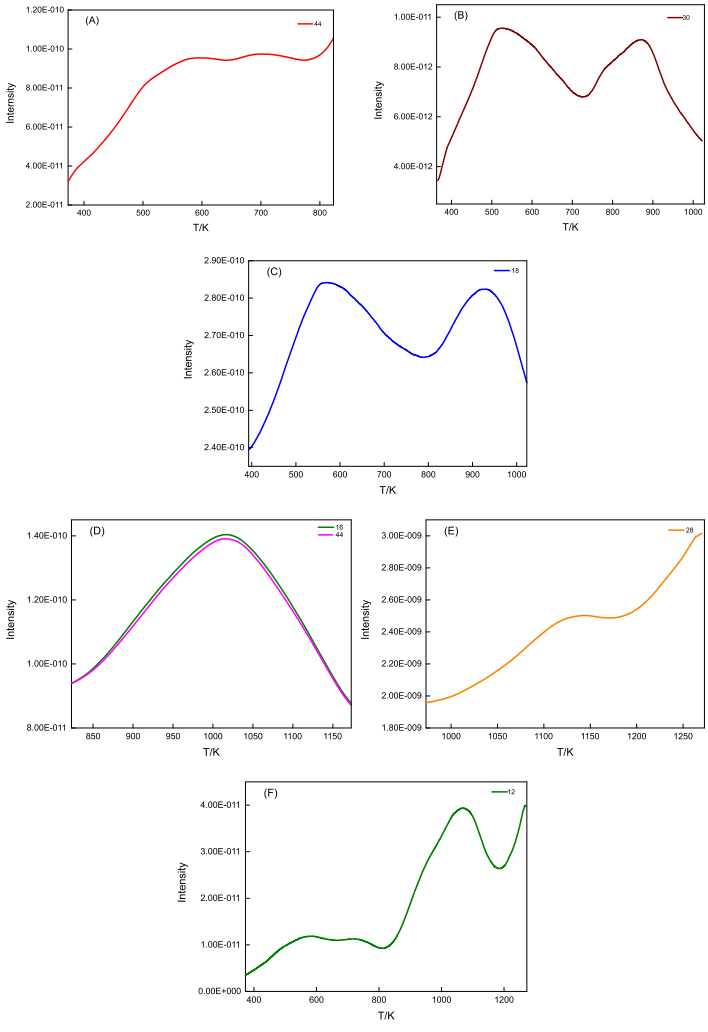

Figure 7. Mass spectrum of major pyrolysis by-products for distillation residues (A), (B), (C), (D), (E) and (F)

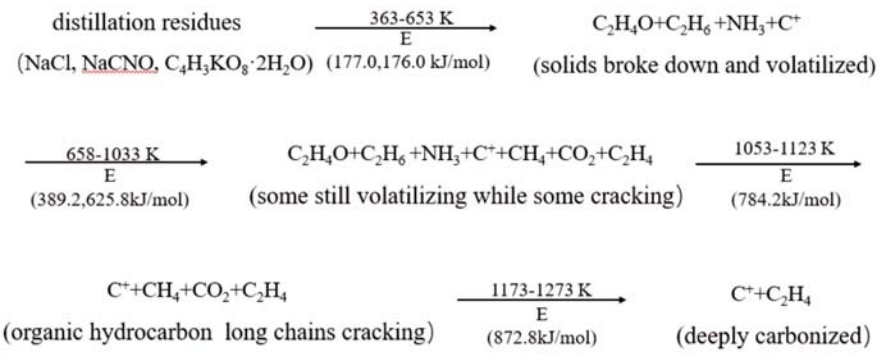

Figure 8. The material pyrolysis path diagram

from 393–1033 K (stage 1, 2, 3, 4). NH_3 (m/z = 18) appeared ranging from 393–1123 K (stage 1, 2, 3, 4) (Fig. 7(C)). Fig. 7(D) displayed that CH_4 (m/z = 16) and CO_2 (m/z = 44) was detected in the temperature range of 843–1123 K (stage 4, 5). C_2H_4 (m/z = 28) appeared at 973 K till the end, and showed an upward trend (stage 5, 6) (Fig. 7(E)). Besides, C^+ (m/z = 12) was monitored in all stages ranging from 393–1273 K and abruptly rose in 843–1273 K (stage 4, 5, 6) (Fig. 7(F)). Based on TG/DTG curves, the pyrolysis path was divided into four stages. Firstly, distillation residues were heated that solids broke down and volatilized some organic matters (stage 1, 2). Secondly, some organics were still volatilizing while some cracking material had been produced (stage 3, 4). Thirdly, organic hydrocarbon chains were formed by material cracking (stage 5). Last, Organic matters were deeply carbonized (stage 6). The material pyrolysis path diagram is shown in Fig. 8. In addition, the analysis of by-product gases indicated that high-temperature treatment technology should be properly improved in corrosion resistance due to the presence of ammonia and the capture, separation and purification of alkanes should be considered at the end of the process highlighting the aim of cleaner production or sustainability, which avoids environmental hazards and maximizes the use of natural resources.

CONCLUSION

In this paper, the effects of full-temperature windows on safe treatments of distillation organic kettle residues were first researched for the aim of cleaner production or sustainability of the biological pharmaceutical factory in China. The possible mechanism of high-temperature degradation of the solid waste was analyzed by the combination of thermal analysis kinetics based on the multi-level comparison ("3-2-2" and "1+1" patterns) and gas by-products online monitoring using TG-MS.

Results presented that the whole pyrolysis process was divided into low and high-temperature zones (six stages) based on characteristics of TG/DTG curves. Stage 1, 3 and 4 were calculated by multiple scanning mode ("3-2-2") and stage 2, 5 and 6 matched single scanning mode ("1+1"). The $E_{(mean)}$ values of the six stages were 177.0, 176.0, 389.16, 625.82, 784.2, and 872.8 kJ/mol, respectively, and the E gradually increased with increasing temperature, indicating that more energy was obtained to break more stable chemical bonds. LgA also showed the same trend due to the dynamic compensation effect ($Lg A_{(mean)}$ = 27.28). "3-2-2" pattern errors were low ranging from 0.06% to 8.56% and the maximum total fluctuation of "1+1" pattern was 33.7 indicating the reliability of the two patterns. Stage 1 and stage 2 could be divided into the initial stage which possibly was the volatilization stage. Stage 3 and 4 are the transition stage, stage 5 may be the cracking stage, and stage 6 may be the carbonization stage. The kinetic triplet of six stages of residues and a possible pyrolysis path at full temperatures windows were presented based on hierarchical comparison using seven models and small molecular gas by-products, which provides the theoretical basis for the establishment of standards involving in high-temperature safe treatment of distillation organic kettle residues.

Acknowledgments

This work was supported by the National Natural Science Foundation (U20A20130, 52004080), the Natural Science Foundation of Hebei Province (B2021208033, E2022208046, B202208020, B2021208040), Hebei Key R&D Program Project (22373704D), Shijiazhuang Key R&D Program Projects (211240233A), Special Project for Cultivating Science and Technology Innovation Ability of College and Middle School Students (22E50079D).

LTERATURE CITED

1. Pieper, M., Kumpert, M., König, B., Schleich, H., Bayer, T. & Gröger, H. (2018). Process development for synthesizing the cephalosporin antibiotic cefotaxime in batch and flow mode. *Org. Process. Res. Dev*., 22, 947–954. DOI: 10.1021/acs.oprd.8b00064.

2. Costa, F., Lago, A., Rocha, V., Barros, O., Costa, L., Vipotnik, Z., Silva, B. & Tavares, T. (2019). A review on biological processes for pharmaceuticals wastes abatement-a growing threat to modern society. *Environ. Sci. Technol*., 53, 7185–7202. DOI: 10.1021/acs.est.8b06977.

3. Wang, Q.H., Zhang, L., Tian, S., Sun, P.T.C. & Xie, W. (2007). A pilot-study on treatment of a waste gas containing butyl acetate, n-butyl alcohol and phenylacetic acid from pharmaceutical factory by bio-trickling filter. *Biochem. Eng. J.*, 37, 42–48.

4. Guo, C., Chen, Y., Chen, J., Wang, X.J., Zhang, G.Q., Wang, J.X., Cui, W.F. & Zhang, Z.Z. (2014). Combined hydrolysis acidification and bio-contact oxidation system with air-lift tubes and activated carbonbioreactor for oilfield wastewater treatment [J]. *Bioresour. Technol.*, 169, 630–636 DOI: 10.1016/j.biortech.2014.07.018.

5. Wu, D., Huang, X.H., Sun, J.Z., Graham, D.W. & Xie, B. (2017). Antibiotic resistance genes and associated microbial community conditions in aging landfill systems. *Environ. Sci. Technol.*, 51, 12859–12867. DOI: 10.1021/acs.est.7b03797.

6. Xu, T., Xu, F., Hu, Z., Chen, Z. & Xiao, B. (2017). Non-isothermal kinetics of biomass-pyrolysis-derived-tar (BPDT) thermal decomposition via thermogravimetric analysis. *Energy. Convers. Manag.*, 138, 452–460. DOI: 10.1016/j.enconman.2017.02.013.

7. Jiang, L., Yuan, X., Li, H., Xiao, Z., Liang, J., Wang, H., Wu, Z., Chen, X. & Zeng, G. (2015). Pyrolysis and combustion kinetics of sludge–camphor pellet thermal decomposition using thermogravimetric analysis. *Energy. Convers. Manag*, 106, 282–289. DOI: 10.1016/j.enconman.2015.09.046.

8. Carrasco, F., Gámez-Pérez, J., Santana, O.O. & Maspoch, M.L. (2011). Processing of poly(lactic acid)/organomontmorillonite nanocomposites: microstructure, thermal stability and kinetics of the thermal decomposition. *Chem. Eng. J*., 178. 451–460. DOI: 10.1016/j.cej.2011.10.036.

9. Hu, Q., Yang, H., Xu, H., Wu, Z., Lim, C.J., Bi, X.T. & Chen, H. (2018).Thermal behavior and reaction kinetics analysis of pyrolysis and subsequent in-situ gasification of torrefied biomass pellets. *Energy. Convers. Manag*., 161, 205–214. DOI: 10.1016/j.enconman.2018.02.003.

10. Wu, D., Li, L., Wang, J.K., Study on decomposition process and thermal analysis kinetics of ammonium sulfate[J/OL]. *Inorganic. Salt. Industry*, 1-13[2023-07-29]. DOI: 10.19964/j.issn.1006-4990.2022-0105.

11. Wu, X.R. & Qiao, J.J. (2023). Combustion process and kinetic analysis of wheat starch[J]. *Chem. Eng. J.*, 51(04), 62–67.

12. Zhu, W., Tian, B., Zhang, X.R. & Zhang, H., Kinetics study on thermal analysis of fischer-tropsch synthetic slag wax[J/OL]. *Clean. Coal. Technology*:1-12[2023-07-29].

13. Salema, A.A., Ting, R.M.W. & Shang, Y.K. (2019). Pyrolysis of blend (oil palm biomass and sawdust) biomass using TG-MS. *Biores. Technol.*, 274, 439–446. DOI: 10.1016/j.biortech.2018.12.014.

14. Song, Y., Hu, J., Liu, J., Evrendilek, F. & Buyukada, M. (2020). Catalytic effects of CaO, Al_2O_3, Fe_2O_3, and red mud on Pteris vittata combustion: emission, kinetic and ash conversion patterns. *J. Clean. Prod.*, 252, 119646.

15. Qiao, Y., Wang, B., Zong, P., Tian, Y., Xu, F., Li, D., Li, F. (2019). Thermal behavior, kinetics and fast pyrolysis characteristics of palm oil: analytical TG-FTIR and Py-GC/MS study. *Energy. Convers. Manag.*, 199, 111964. DOI: 10.1016/j.enconman.2019.111964.

16. Yi, H., Yang, Z., Tang, X., Zhao, S., Gao, F., Wang, J., Huang, Y., Yang, K., Shi, Y. & Xie, X. (2018). Variations of apparent activation energy based on thermodynamics analysis of zeolitic imidazolate frameworks including pyrolysis and combustion. *Energy*, 151, 782–798. DOI: 10.1016/j.energy.2018.03.107.

17. Ren, D., Liu, X., Feng, X., Lu, L., Ouyang, M., Li, J. & He, X. (2018). Model-based thermal runaway prediction of lithium-ion batteries from kinetics analysis of cell components. *Appl. Energy*, 228, 633–644. DOI: 10.1016/j.apenergy.2018.06.126.

18. Liu, J., Huang, L., Xie, W., Kuo, J., Buyukada, M. & Evrendilek, F. (2019). Characterizing and optimizing (CO-) pyrolysis as a function of different feedstocks, atmospheres, blend ratios, and heating rates. *Bioresour. Technol.*, 277, 104–116. DOI: 10.1016/j.biortech.2019.01.003.

19. Zou, H., Li, W., Liu, J., Buyukada, M. & Evrendilek, F. (2020). Catalytic combustion performances, kinetics, reaction mechanisms and gas emissions of lentinus edodes. *Bioresour. Technol.*, 300, 122630. DOI: 10.1016/j.biortech.2019.122630.

20. Huang, J., Liu, J., Kuo, J., Xie, W., Zhang, X., Chang, K., Buyukada, M. & Evrendilek, F. (2019). Kinetics, thermodynamics, gas evolution and empirical optimization of (CO-) combustion performances of spent mushroom substrate and textile dyeing sludge. *Bioresour. Technol.*, 280, 313–324. DOI: 10.1016/j.biortech.2019.02.011.

21. Zhang, J., Liu, J., Evrendilek, F., Zhang, X. & Buyukada, M. (2019). TG-FTIR and Py-GC/MS analyses of pyrolysis behaviors and products of cattle manure in CO_2 and N_2 atmospheres: kinetic, thermodynamic, and machine-learning models. *Energy. Convers. Manag.*, 195, 346–359. DOI: 10.1016/j.enconman.2019.05.019.

22. Hu, J., Song, Y., Liu, J., Evrendilek, F., Buyukada, M., Yan, Y. & Li, L. (2020). Combustions of torrefaction-pretreated bamboo forest residues: physicochemical properties, evolved gases, and kinetic mechanisms. *Biores. Technol.*, 304, 122960. DOI: 10.1016/j.biortech.2020.122960.

23. Cai, H., Liu, J., Xie, W., Kuo, J., Buyukada, M. & Evrendilek, F. (2019). Pyrolytic kinetics, reaction mechanisms and products of waste tea via TG-FTIR and Py-GC/MS. *Energy. Convers. Manag.*, 184, 436–447. DOI: 10.1016/j.enconman.2019.01.031.

24. Liu, Z.G., Wang, Z., Tang, J., Wang, H.T. & Long, H.M. (2015). Non-isothermal thermal decomposition kinetics of high iron gibbsite ore based on popescu method. *T. Nonferr. Metal. Soc.*, 25, 2415–2421. DOI: 10.1016/S1003-6326(15)63857-2.

25. He, Q., Ding, L., Gong, Y., Li, W., Wei, J. & Yu, G. (2019). Effect of torrefaction on pinewood pyrolysis kinetics and thermal behavior using thermogravimetric analysis. *Bioresour. Technol.*, 280, 104–111. DOI: 10.1016/j.biortech.2019.01.138.

26. Biasin, A., Fabro, J., Michelon, N., Glisenti, A. & Canu, P. (2019). Investigation of thermal effects on heterogeneous exothermic reactions and their impact on kinetics studies. *Chem. Eng. J.*, 377, 120179. DOI: 10.1016/j.cej.2018.10.116.

27. Yang, Z., Zhang, L., Zhang, Y., Bai, M., Zhang, Y., Yue, Z. & Duan, E. (2020). Effects of apparent activation energy in pyrolytic carbonization on the synthesis of MOFs-carbon involving thermal analysis kinetics and decomposition mechanism. *Chem. Eng. J.*, 395, 124980. DOI: 10.1016/j.cej.2020.124980.

28. Yang, Z., Yi, H., Tang, X., Zhao, S., Yu, Q., Gao, F., Zhou, Y., Wang, J., Huang, Y., Yang, K. & Shi, Y. (2017). Potential demonstrations of "hot spots" presence by adsorption-desorption of toluene vapor onto granular activated carbon under microwave radiation. *Chem. Eng. J.*, 319, 191–199. DOI: 10.1016/j.cej.2017.02.157.

29. Zhu, D., Huang, Y., Cao, J.J., Lee, S.C., Chen, M. & Shen, Z. (2019). Cobalt nanoparticles encapsulated in porous nitrogen-doped carbon: oxygen activation and efficient catalytic removal of formaldehyde at room temperature. *Appl. Catal. B*, 258, 117981. DOI: 10.1016/j.apcatb.2019.117981.

30. Marpaung, F., Kim, M., Khan, J.H. (2019). Konstantinov, K., Yamauchi, Y., Hossain, M.S.A., Na, J. & Kim, J., Metal-organic framework (MOF)-derived nanoporous carbon materials, *Chem. Asian. J.*, 14, 1331–1343. DOI: 10.1002/asia.201900026.

31. Zhang, J.X., Zhou, L.N., Cheng, J., Yin, X., Kuang, W.T. & Li, Y.J. (2019). CoII-catalyzed room-temperature growth of MnO_2 on the skeleton of carbonized zeolitic imidazolate framework-67 crystals for boosting oxygen reduction reaction. *J. Mater. Chem. A*, 7, 4699–4704. DOI: 10.1039/C8TA11658J.

32. Jaria, G., Lourenço, M.A.O., Silva, C.P., Ferreira, P., Otero, M., Calisto, V. & Esteves, V.I. (2020). Effect of the surface functionalization of a waste-derived activated carbon on pharmaceuticals' adsorption from water. *J. Mol. Liq.*, 29,9, 112098. DOI: 10.1016/j.molliq.2019.112098.

33. Silva, C.P., Jaria, G., Otero, M., Esteves, V.I. & Calisto, V. (2018). Waste-based alternative adsorbents for the remediation of pharmaceutical contaminated waters: Has a step forward already been taken? *Biores. Technol.*, 250, 888–901. DOI: 10.1016/j.biortech.2017.11.102.

34. Yamuna Rani, M., Bhagawan, D., Himabindu, V., Venkateswara Reddy, V. & Saritha, P. (2016). Preparation and characterization of green bricks using pharmaceutical industrial wastes. *Environ. Sci. Pollut. Res.*, 23, 9323–9333. DOI: 10.1007/s11356-015-5191-2.

35. Klejnowska, K., Pikon, K., Scierski, W., Skutil, K., Bogacka, M. (2020). Influence of temperature on the composition and calorific value of gases produced during the pyrolysis of waste pharmaceutical blisters. *Appl. Sci.*, 737, 1–10. DOI: 10.3390/app10030737.